



## Article

# An Open-Pit Mines Land Use Classification Method Based on Random Forest Using UAV: A Case Study of a Ceramic Clay Mine

Yuanrong He <sup>1,2,3</sup>, Yangfeng Lai <sup>1,3,\*</sup> , Bingning Chen <sup>3</sup>, Yuhang Chen <sup>1,3</sup> , Zhiying Xie <sup>1,2,3</sup>, Xiaolin Yu <sup>1</sup> and Min Luo <sup>3</sup>

<sup>1</sup> Digital Fujian Institute of Big Data for Natural Disaster Monitoring, Xiamen University of Technology, Xiamen 361024, China

<sup>2</sup> Hunan Key Laboratory of Remote Sensing Monitoring of Ecological Environment in Dongting Lake Area, Changsha 410004, China

<sup>3</sup> School of Computer and Information Engineering, Xiamen University of Technology, Xiamen 361024, China

\* Correspondence: 2222031120@stu.xmut.edu.cn

**Abstract:** Timely and accurate land use information in open-pit mines is essential for environmental monitoring, ecological restoration planning, and promoting sustainable progress in mining regions. This study used high-resolution unmanned aerial vehicle (UAV) imagery, combined with object-oriented methods, optimal segmentation algorithms, and machine learning algorithms, to develop an efficient and practical method for classifying land use in open-pit mines. First, six land use categories were identified: stope, restoration area, building, vegetation area, arterial road, and waters. To achieve optimal scale segmentation, an image segmentation quality evaluation index is developed, emphasizing both high intra-object homogeneity and high inter-object heterogeneity. Second, spectral, index, texture, and spatial features are identified through out-of-bag (OOB) error of random forest and recursive feature elimination (RFE) to create an optimal multi-feature fusion combination. Finally, the classification of open-pit mines was executed by leveraging the optimal feature combination, employing the random forest (RF), support vector machine (SVM), and k-nearest neighbor (KNN) classifiers in a comparative analysis. The experimental results indicated that classification of appropriate scale image segmentation can extract more accurate land use information. Feature selection effectively reduces model redundancy and improves classification accuracy, with spectral features having the most significant effect. The RF algorithm outperformed SVM and KNN, demonstrating superior handling of high-dimensional feature combinations. It achieves the highest overall accuracy (OA) of 90.77%, with the lowest misclassification and omission errors and the highest classification accuracy. The disaggregated data facilitate effective monitoring of ecological changes in open-pit mining areas, support the development of mining plans, and help predict the quality and heterogeneity of raw clay in some areas.

**Keywords:** UAV; object-oriented; random forest; open-pit mines; land use classification



**Citation:** He, Y.; Lai, Y.; Chen, B.; Chen, Y.; Xie, Z.; Yu, X.; Luo, M. An Open-Pit Mines Land Use Classification Method Based on Random Forest Using UAV: A Case Study of a Ceramic Clay Mine. *Minerals* **2024**, *14*, 1282. <https://doi.org/10.3390/min14121282>

Academic Editor: Konstantinos G. Nikolakopoulos

Received: 19 November 2024

Revised: 12 December 2024

Accepted: 14 December 2024

Published: 17 December 2024



**Copyright:** © 2024 by the authors. Licensee MDPI, Basel, Switzerland. This article is an open access article distributed under the terms and conditions of the Creative Commons Attribution (CC BY) license (<https://creativecommons.org/licenses/by/4.0/>).

## 1. Introduction

Open-pit mines are crucial for economic development, but excessive exploration has led to concerns over ecological degradation, environmental pollution, and geological disasters [1]. Therefore, efficiently and accurately capturing mine land use information holds significant importance. Unlike urban, forest, and farmland, land use in mining areas is subject to frequent changes, often accompanied by significant geomorphic alterations such as excavation, accumulation, and subsidence [2,3]. Thus, extracting this information has been a technical challenge. Traditional surveying and mapping technologies are constrained by manual dependence, high cost, and limited timeliness in acquiring mine land use information [4]. Remote sensing technology provides fast, accurate, and large-scale analysis using multi-temporal, multispectral, and multiresolution data [5]. It has become

an important tool for understanding the ecological dynamics and resource exploitation in mining regions.

In the past decade, due to its rapid advancement, remote sensing technology has garnered significant attention in land information extraction research. Satellite multispectral imagery is used as the basic data for land use information extraction [6,7]. For example, Myint et al. [8] utilized QuickBird satellite imagery to assess object-oriented classification methods in Phoenix, Arizona, demonstrating significant improvements in classification precision, attributable to object-oriented analytical approaches. Akar et al. [9] utilized airborne hyperspectral imagery and machine learning algorithms such as RF and SVM for land use/land cover mapping. The study revealed that incorporating Gabor texture information into machine learning enhanced the classification accuracy by 9%. Hu et al. [10] proposed the Multi-scale Land Use Multi-classification Network model, a land use classification method based on remote sensing imagery. The model eliminates the influence of data category occupancy ratio, improves the structural integrity of land parcels, refines the classification boundaries, and enhances the overall classification accuracy. However, satellite remote sensing imagery suffers from high data acquisition costs, susceptibility to severe weather conditions, and spatial resolution limitations, posing difficulty for extracting small-scale mining regions. Mitchell et al. [11] noted that the spatial resolution of satellite remote sensing is insufficient, making it difficult to achieve high-precision land cover mapping. Shaik et al. [12] utilized the high-resolution images from the PRISMA satellite for remote sensing mapping, but the susceptibility to atmospheric interference remains a significant problem. Further investigation is required to address the limitations of satellite imagery and to enhance the accuracy of land use information extraction.

UAV remote sensing technology has rapidly advanced, offering advantages of simple operation, easy image acquisition, high spatial resolution, and low weather dependence [13]. These attributes address the limitations often encountered with satellite remote sensing. The utilization of UAV images in land use classification offers abundant spectral, index, texture, and spatial features, facilitating efficient extraction of land use data. Fu et al. [14] employed high-resolution UAV imagery to monitor land use dynamics, overcoming problems associated with satellite image acquisition in cloudy and foggy mountainous areas. Zhang et al. [15] applied an improved DeepLabv3+\_BA model to classify land use information in UAV images of the Weibei Plateau in China, achieving good results.

Machine learning and deep learning have yielded fruitful results in land use classification [16], yet their combined use with UAV imagery for open-pit mine classification remains rare. In addition, the mixed pixels in mine area images contain a wide range of complex primitives [17], complicating accurate and efficient information extraction in mine areas using current methods. This study uses high-resolution UAV imagery to construct a segmentation quality evaluation index model to achieve optimal segmentation scale. The influence of various feature categories on classification outcomes is analyzed, and the optimal feature combination is obtained using RFE. On this basis, RF algorithm classification was determined, aiming to obtain an open-pit mines land use classification method based on UAV imagery.

The mining activities continue unabated, with concurrent dynamic changes in land use patterns. UAV aerial photography, leveraging its efficient imaging capabilities, enables the rapid acquisition and classification of mine imagery, thereby facilitating real-time tracking and monitoring of land use conditions in mining areas. This study innovatively applies high-resolution UAV imagery to the extraction of land information in open-pit mines. The proposed segmentation quality evaluation index model and multi-feature optimization method hold significant applied value, providing a valuable reference for subsequent monitoring, management, and protection of open-pit mines.

## 2. Materials and Methods

### 2.1. Study Area

The study area, positioned at coordinates (118°42' E, 26°07' N), is found in Minqing County, Fuzhou City, Fujian Province, China, and is depicted in Figure 1. The area is a typical estuary basin surrounded by mountains, with an overall terrain sloping from west to east and an elevation between 600 and 1000 m [18]. The study area is a ceramic clay mine, which is mainly formed by hydrothermal alteration of rhyolite host rock, with uneven and locally intense alteration. The mine area is hilly, and long-term mining has led to large topographic slopes, with some side slopes up to 75°.

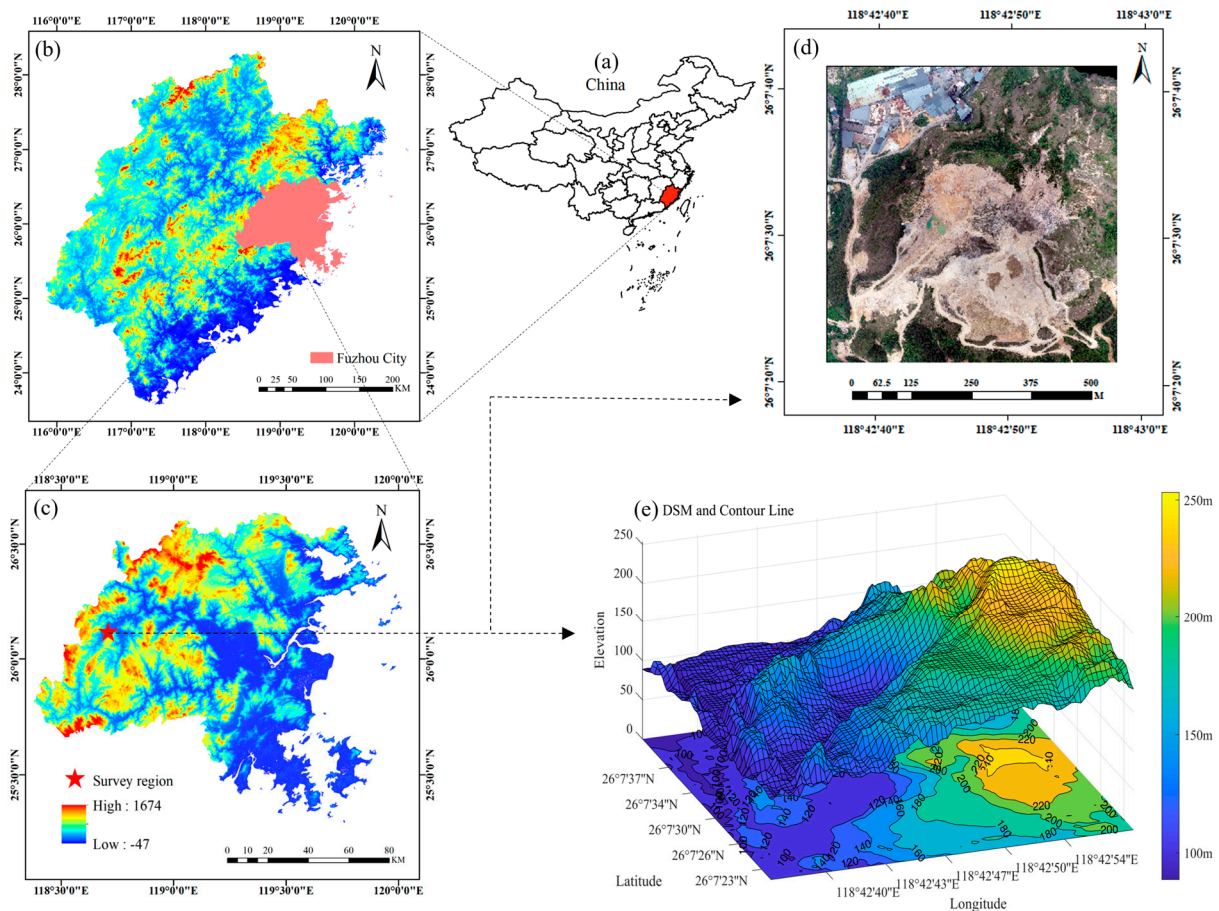


**Figure 1.** Study area: (a–c) location of the study area in China, Fujian province, and Fuzhou city, respectively. The base map of (b) and (c) is a digital elevation model. (d) The orthophoto and (e) the digital surface model of the study area.

### 2.2. Data Acquisition and Preprocessing

The data were acquired by the DJI M300RTK UAV (Da-Jiang Innovations, Shenzhen, China) in May 2023, under clear weather conditions with high visibility, resulting in high-quality images. The drone captured true-color images containing red ( $700 \pm 16$  nm), green ( $550 \pm 16$  nm), and blue ( $450 \pm 16$  nm) bands. An aggregate of 262 images was acquired, each with a size of  $5471 \times 3648$  pixels, and the imagery yielded a spatial resolution of roughly 0.04 m. These images were used to generate a three-dimensional (3D) model through aerial triangulation, dense cloud generation, and 3D reconstruction using ContextCapture software (v4.4.10, Bentley Systems, Exton, PA, USA). To enhance the accuracy of data within the study area, this research employed an alignment model method. Using the 3D model as a reference, the distances between three image control points (P1, P2, and P3) in different orientations on the model were measured. Com-

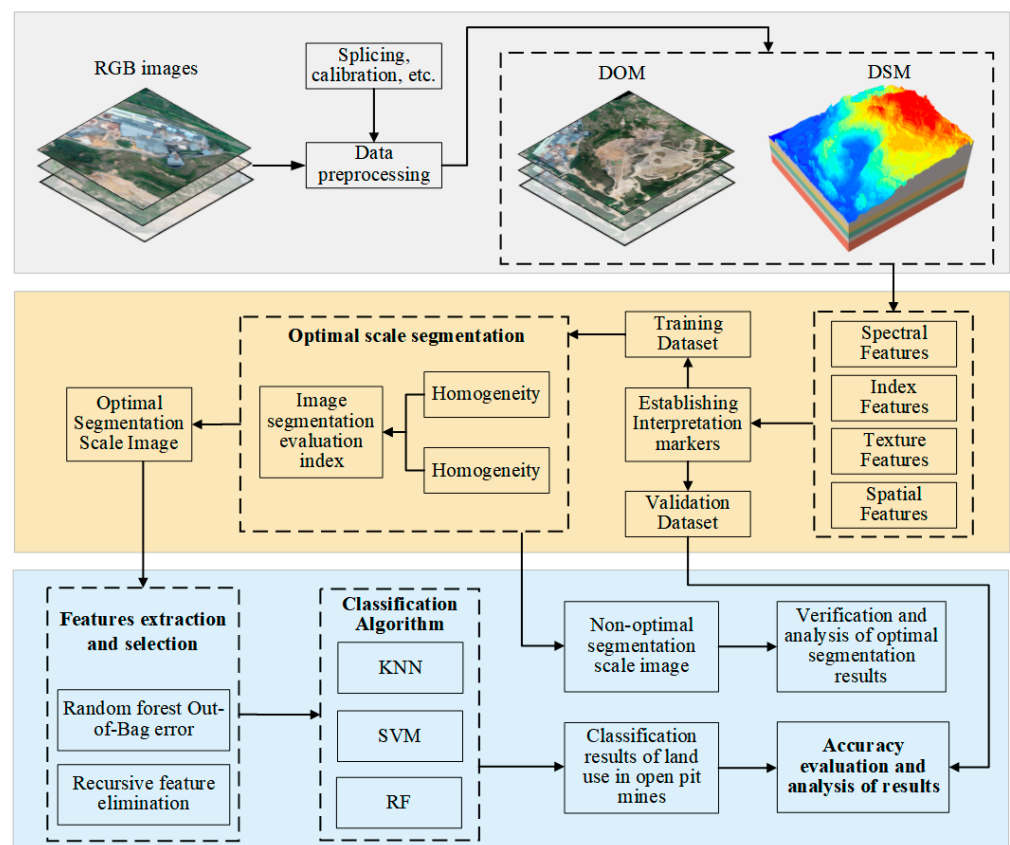
bined with the field tape measurement data on the day of the UAV aerial photography, the scaling coefficient of the model was calculated (see Table 1) and finally determined to be 1.046. Then the 3D model was enlarged by 1.046 times to improve the accuracy of spatial matching, and the optimized digital orthophoto map (DOM) and digital surface model (DSM) were derived (Figure 1d,e).

**Table 1.** Calculation of scaling coefficient.

Image Control Point Identification	On-Site Measurement	Model Measurement	Scaling Factor	Overall Scaling Coefficient
P1 to P2	119.53 m	113.95 m	1.049	1.046
P1 to P3	85.78 m	82.16 m	1.044	
P2 to P3	107.66 m	102.93 m	1.046	

2.3. Research Methods

This study proposes a land use classification method for open-pit mines, utilizing visible imagery captured by unmanned aerial vehicles (UAVs) employing an object-oriented method combined with machine learning algorithms. The classification method has five key stages (Figure 2): (1) optimal scale segmentation, involving image segmentation evaluation index construction, optimal split-scale determination, and image segmentation; (2) features extraction and selection, using ENVI for image feature extraction and using OOB error of RF and recursive feature elimination to select an optimal feature combination; (3) classification implementation, where open-pit mines are classified using RF, SVM, and KNN algorithms; (4) accuracy evaluation, where the accuracy of the classification results is assessed by metrics such as user accuracy (UA), producer accuracy (PA), OA, and Kappa; and (5) analysis of classification results.

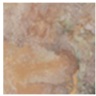
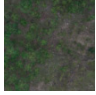
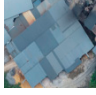
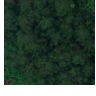




**Figure 2.** Flowchart of this research.

### 2.3.1. Establish Interpretation Markers

Through field surveys and image analysis, the mining area was divided into six distinct categories: stope, restoration area, building, vegetation area, arterial road, and waters (Table 2). A total of 390 samples were collected, including 96 stopes, 138 restoration areas, 36 buildings, 86 vegetation areas, 30 arterial roads, and 4 waters. From the sample points of each land category, 50% were designated for training, and the other 50% were assigned for validation.

**Table 2.** Images and characteristics of the land use categories in open-pit mines.

Land Use Categories	Image	Characteristics
Stope		Lower than the surrounding terrain, with little vegetation cover, significantly different from the surrounding area in hue and texture, with irregular shapes.
Restoration area		Grayish-green tones, low vegetation, coarse texture, scattered distribution, brighter than vegetation, irregular shape.
Building		Some areas show continuous cluster distribution, most featuring shift buildings with blue and brown iron shed roofs; some concrete structures have gray roofs with regular shapes.
Vegetation area		Green, tall vegetation with scattered distribution, lower brightness than restoration area, irregular shape.
Arterial road		Grayish white, high brightness, adjacent to stopes and buildings, boundary with steps, long and narrow in shape.
Waters		Blue-green, low brightness, small spectral standard deviation, irregular shape.

### 2.3.2. Image Segmentation

Recently, there has been an increasing tendency to use object-oriented methods for classifying remote sensing images. Selecting an appropriate segmentation scale is critical for maintaining object homogeneity while preserving inter-object heterogeneity [19]. A larger scale may lead to under-segmentation, compromising accuracy and integrity, while a smaller scale may result in over-segmentation, disrupting the image's continuity [20]. This study constructs a global segmentation quality evaluation index to balance homogeneity and heterogeneity. Higher evaluation values indicate better segmentation quality. The detailed procedure is outlined below:

1. The images were segmented using eCognition Developer 10.3 software across multiple scales. The study area was segmented 33 times at scales of 100~400 with a step size of 20.
2. The intra-object homogeneity evaluation index  $V$  was calculated by area and standard deviation [21], as follows:

$$V = \frac{\sum_{i=1}^n a_i v_i}{\sum_{i=1}^n a_i} \quad (1)$$

In which  $n$  is the overall count of segmented image objects;  $v_i$  is the standard deviation of element  $i$ ; and  $a_i$  is the area of element  $i$ .

3. The heterogeneity between objects is assessed by the global Moran index ( $I_M$ ) in the literature [22], as follows:

$$I_M = \frac{n \sum_{i=1}^n \sum_{j=1}^n w_{ij} (y_i - \bar{y})(y_j - \bar{y})}{\left(\sum_{i=1}^n (y_i - \bar{y})^2\right) \left(\sum_{i \neq j} \sum w_{ij}\right)} \tag{2}$$

In which  $n$  is the total count of elements;  $W_{ij}$  is the spatial weighting factor associated with elements  $i$  and  $j$ , where  $W_{ij} = 1$  if the elements are adjacent, and 0 otherwise;  $y_i$  is the spectral mean of element  $i$ .

4. Homogeneity  $V$  and heterogeneity  $I_M$  are normalized as follows:

$$V_{norm}(I_{Mnorm}) = \frac{X - X_{min}}{X_{max} - X_{min}} \tag{3}$$

In which  $X$  is the value of  $V$  ( $I_M$ ) in a certain scale;  $X_{max}$  and  $X_{min}$  are the maximum and minimum values of  $V$  ( $I_M$ ) for all partition scales.

5. Combining  $V_{norm}$  and  $I_{Mnorm}$ , the image segmentation quality evaluation index  $GS$  is obtained:

$$GS = \sum_{i=1}^n \frac{V_{norm} + I_{Mnorm}}{n} \tag{4}$$

In which  $n$  is the count of image bands, and  $V_{norm}$  and  $I_{Mnorm}$  are calculated from Equation (3). The smaller the  $GS$  value, the higher the segmentation quality.

### 2.3.3. Classification Feature Extraction

A total of 58 features were extracted from the objects, as detailed in Table 3.

**Table 3.** Feature list.

Feature Types	Feature Variables	Feature Count
Spectral features	Mean_R, Mean_G, Mean_B, SD_R, SD_G, SD_B, Brightness, Max_diff	8
Index features	RGRI, NGRDI, EXG, RGBVI, VDVl	5
Texture features	GLCM_Mean1, GLCM_Mean2, GLCM_Mean3, GLCM_Mean4, GLCM_SD1, GLCM_SD2, GLCM_SD3, GLCM_SD4, GLCM_Ctrst1, GLCM_Ctrst2, GLCM_Ctrst3, GLCM_Ctrst4, GLCM_Dis1, GLCM_Dis2, GLCM_Dis3, GLCM_Dis4, GLCM_Hom1, GLCM_Hom2, GLCM_Hom3, GLCM_Hom4, GLCM_Ent1, GLCM_Ent2, GLCM_Ent3, GLCM_Ent4, GLCM_Cor1, GLCM_Cor2, GLCM_Cor3, GLCM_Cor4, GLCM_Asm1, GLCM_Asm2, GLCM_Asm3, GLCM_Asm4	32
Spatial features	Elevation, slope, aspect, area, length, width, length/width, pixels, Bord_Index, Shp_Index, asymmetry, compactness, density	13

1. Spectral features include mean or standard deviation (SD) of the visible light bands (red, green, and blue), maximum difference (Max\_diff), and brightness, totaling 8 [23].
2. Index features include the red-green ratio index (RGRI), the normalized green-red difference index (NGRDI), the excess green index (EXG), the red-green-blue vegetation index (RGBVI), and the visible-band difference vegetation index (VDVI), totaling 5. The formula for calculating the vegetation index is presented in Table 4.

Index features can enhance the spectral differences between different land cover types and reduce the influence of atmospheric, light, and other environmental factors, thereby improving the accuracy of classification. The ENVI5.6 software was used to calculate the above vegetation indices. The outcomes are shown in Figure 3.

Table 4. Visible vegetation index.

Vegetation Index	Calculation Formula	Theoretical Interval	Reference
RGRI	$RGRI = \frac{R}{G}$	[0,255]	[24]
NGRDI	$NGRDI = \frac{G-R}{G+R}$	[-1,1]	[25]
EXG	$EXG = 2G - R - B$	[-255,510]	[26]
RGBVI	$RGBVI = \frac{G^2 - (R \times B)}{G^2 + (R \times B)}$	[-1,1]	[27]
VDVI	$VDVI = \frac{2G - R - B}{2G + R + B}$	[-1,1]	[28]

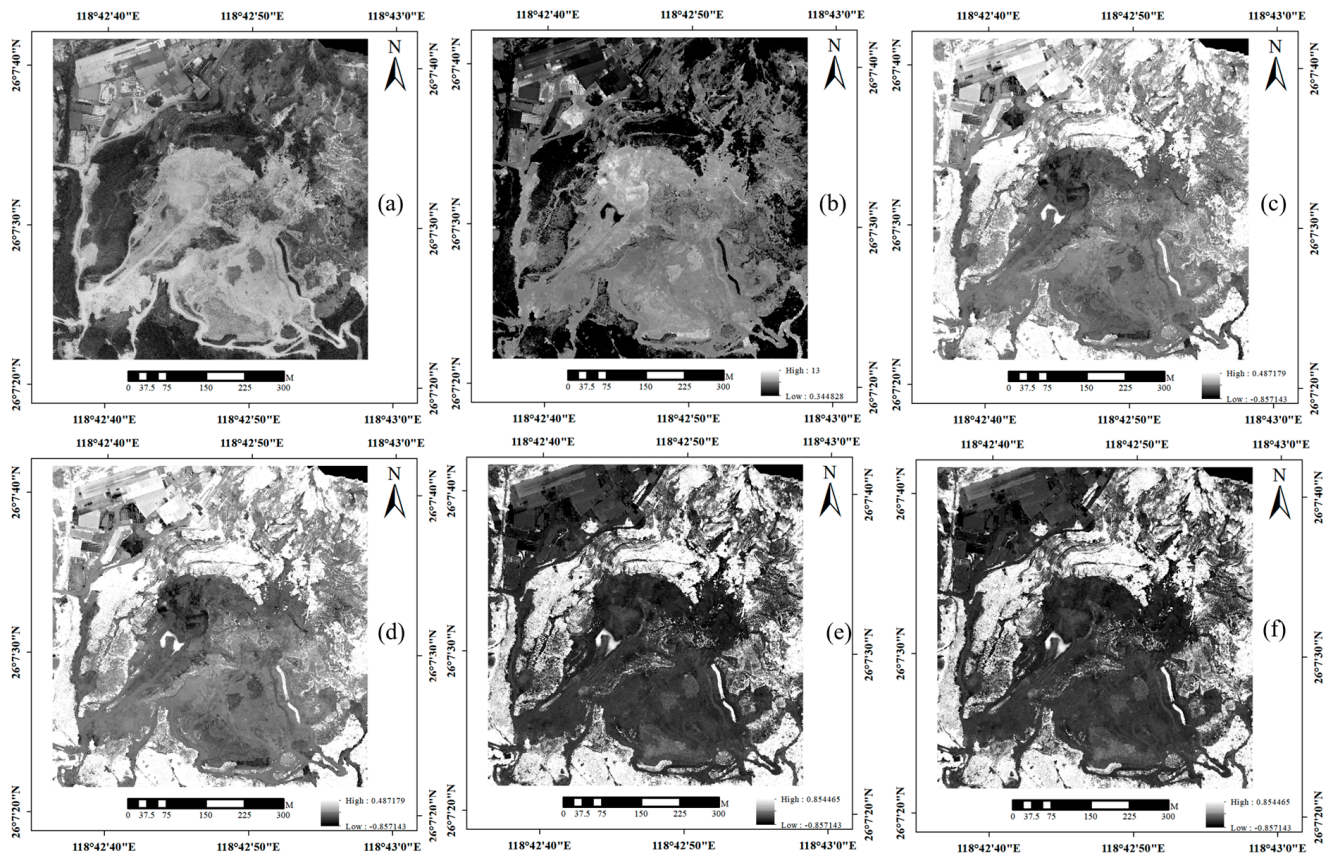


**Figure 3.** Original image and visible vegetation index image: (a) original image, (b) RGRI image, (c) NGRDI image, (d) EXG image, (e) RGBVI image, (f) VDVI image. (b, c, d, e, and f were calculated using ENVI software, version 5.6).

- Texture features were extracted by the gray-level co-occurrence matrix (GLCM) methodology. A total of 32 texture features were selected from four directions ( $0^\circ$ ,  $45^\circ$ ,  $90^\circ$ , and  $135^\circ$ ), numbered 1 to 4 in order, and eight categories: mean, standard deviation, contrast (Ctrst), dissimilarity (Dis), homogeneity (Hom), entropy (Ent), correlation (Cor), and angular second moment (Asm).
- Spatial features include object shape features and range features, totaling 13.

#### 2.3.4. Feature Selection

When processing data, using all features for classification can lead to information redundancy and the “curse of dimensionality” [29,30]. To address this, this study first used the OOB error of RF to assess feature importance. Following this, the RFE method was employed to determine the optimal number of features and construct the optimal feature combination for land use classification in open-pit mines. In the classification task, each decision tree predicts independently, and the object’s classification is determined by majority voting [31]. The OOB error is also used to evaluate feature impor-

tance and misclassification rate. The significance of feature  $F$  is determined using the following formula:

$$F_{\text{imp}} = \frac{\sum_{n=1}^N (OOB_n - OOB_0)}{N} \tag{5}$$

where  $OOB_n$  is the  $OOB$  error of the  $n$ th decision tree after adding noise interference to feature  $F$ ;  $OOB_0$  is the  $OOB$  error of the  $n$ th decision tree before adding noise interference;  $N$  is the number of decision trees.

RFE is an iterative machine learning technique for feature selection that operates. It removes the least important features and retrains the model until achieving the optimal feature combination [32]. By decreasing the feature count, RFE enhances the predictive capability of the model. RFE is especially effective when combined with the RF algorithm.

### 2.3.5. Classification Algorithm

Many methods have been proposed for classifying remote sensing imagery, and the choice between supervised or unsupervised classification depends on the availability of prior knowledge [33]. Object-oriented classification methods effectively utilize the spectral, index, texture, and spatial features of high-resolution UAV imagery to enhance classification precision. In this study, the randomForest, e1071, and class packages of the R language are used as the RF, SVM, and KNN algorithms, respectively [34].

1. RF uses a majority voting method to obtain prediction results through bootstrapping and a feature random selection strategy. The RF flowchart is shown in Figure 4. RF performs well in regression and classification tasks, offering robustness, anti-overfitting ability, and efficient parallel processing capabilities [35]. Bootstrapping is the process of training different subsets of the dataset simultaneously using different decision trees, ensuring that each decision tree in the RF model is unique, thus increasing the diversity and generalization ability of the model [36,37]. As the number of decision trees in the random forest increases, the misclassification rate decreases sharply before stabilizing. When the number of trees reaches around 500, the misclassification rate stabilizes. Therefore, the number of trees is set to 500 for training the random forest model, and the number of features for classification nodes was determined to be the square root of the total number of features.

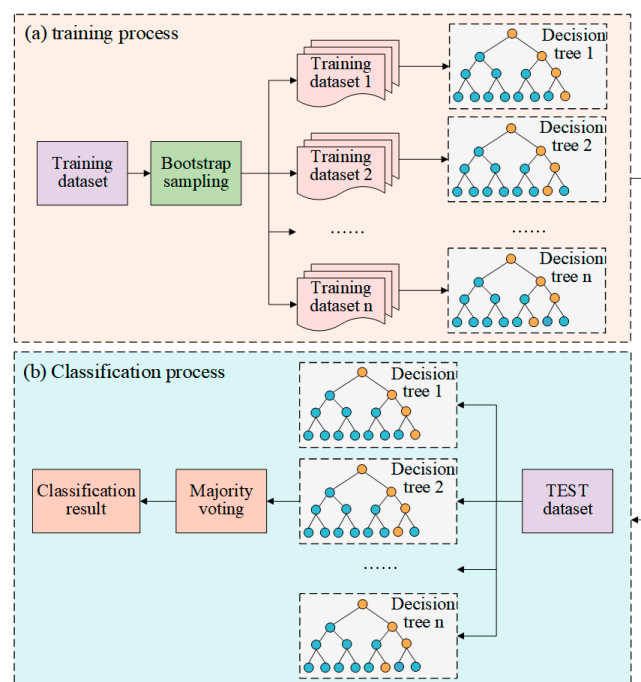


Figure 4. Random forest algorithm.



- SVM operates on the principles of minimizing structural risk and is grounded in statistical learning theory [38]. SVM has strong generalization ability and is suitable for high-dimensional, nonlinear problems and small sample scenarios. This study uses an SVM algorithm with a radial basis function kernel for land use classification to reduce computational costs and prevent the “curse of dimensionality” [39]. The SVM flowchart is shown in Figure 5.

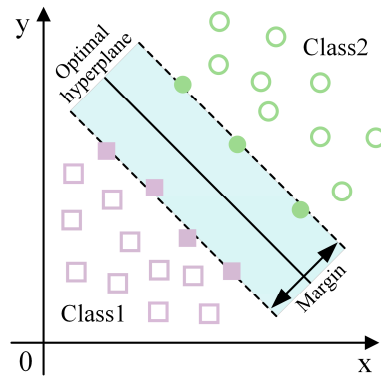


Figure 5. Support vector machine algorithm.

- KNN is a traditional supervised learning algorithm, and its core principle is that objects are assigned to the majority category of the  $k$  nearest objects in feature space [40]; the KNN flowchart is shown in Figure 6. The KNN algorithm was used in this study to take advantage of its lack of prior assumptions in dealing with different datasets and its robustness to outliers. Compared to the traditional nearest neighbor method, KNN reduces sensitivity to outliers and noisy data, thereby improving classification accuracy [41].

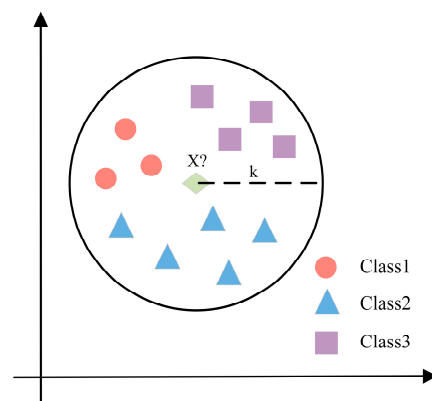


Figure 6. K-nearest neighbor algorithm.

### 2.3.6. Classification Accuracy Evaluation

The UA [42], PA [42], OA [43], and Kappa [43] are utilized to evaluate the classification accuracy of the models. UA represents the percentage of accurately categorized items relative to the overall count of specific objects, whereas PA represents the ratio of the number of correctly classified objects of a certain land category to the total number of land use categories. These metrics are calculated from the confusion matrix and provide an extensive evaluation of the model’s performance. The formulas are as follows:

$$UA = \frac{P_{ii}}{P_{i+}} \times 100\% \tag{6}$$

$$PA = \frac{P_{ii}}{P_{+i}} \times 100\% \tag{7}$$

$$OA = \frac{\sum_{i=1}^n P_{ii}}{P} \times 100\% \tag{8}$$

$$Kappa = \frac{P \sum_{i=1}^n P_{ii} - \sum_{i=1}^n (P_{i+} P_{+i})}{P^2 - \sum_{i=1}^n (P_{i+} P_{+i})} \tag{9}$$

In the formula,  $P_{ii}$  represents the total number of samples correctly classified as land use information in category  $i$ ;  $P_{i+}$  represents the total number of the  $i$ -th row of the confusion matrix, corresponding to the  $i$ -th class of features in the prediction sample;  $P_{+i}$  represents the total number of the  $i$ -th column, corresponding to the sum of the  $i$ -th class of features in the validation sample;  $n$  represents the number of land use categories; and  $P$  represents the total number of samples.

### 3. Results and Analysis

#### 3.1. Segmentation Parameter Determination

The efficacy of object-oriented land use classification is intimately correlated with the quality of image segmentation. As shown in Figure 7, within the segmentation scale range of 100 to 400, the segmentation quality evaluation index ( $GS$ ) demonstrates an initial increase followed by a decrease and then a subsequent increase. The peak value occurs between 280 and 320. When the scale is less than 200, over-segmentation occurs, which slows down calculation. When the scale is greater than or equal to 340, under-segmentation occurs, meaning that different land features were merged into a single object. The lowest point appeared at a scale of 280, registering a  $GS$  of 0.9553, showing minimal difference compared to the value at a scale of 300. To improve classification accuracy, additional experiments were conducted at scales of 285, 290, and 295. The optimal segmentation scale was finally determined to be 285, where  $GS$  reached the lowest value of 0.9242, signifying the optimal segmentation result. Taking into account the shape and distribution of land categories within the study area, the shape factor and compactness were adjusted to 0.2 and 0.6, respectively.

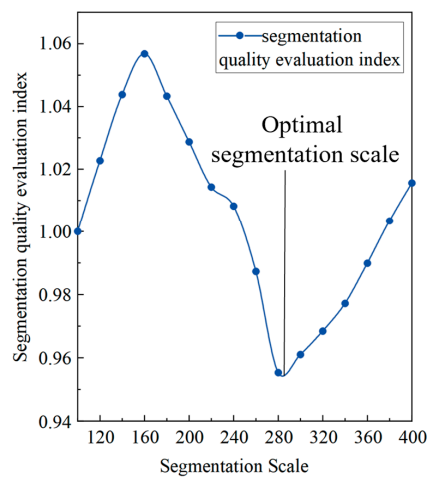
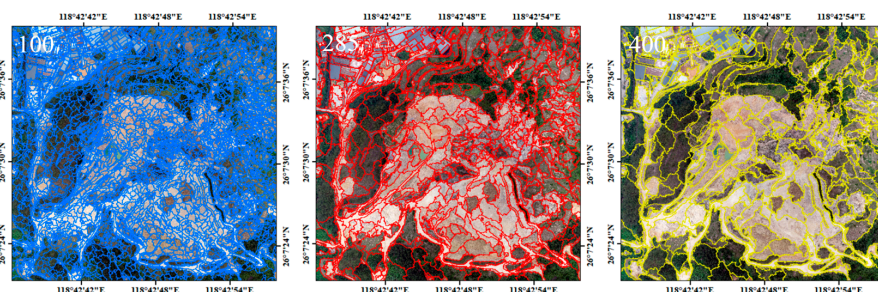
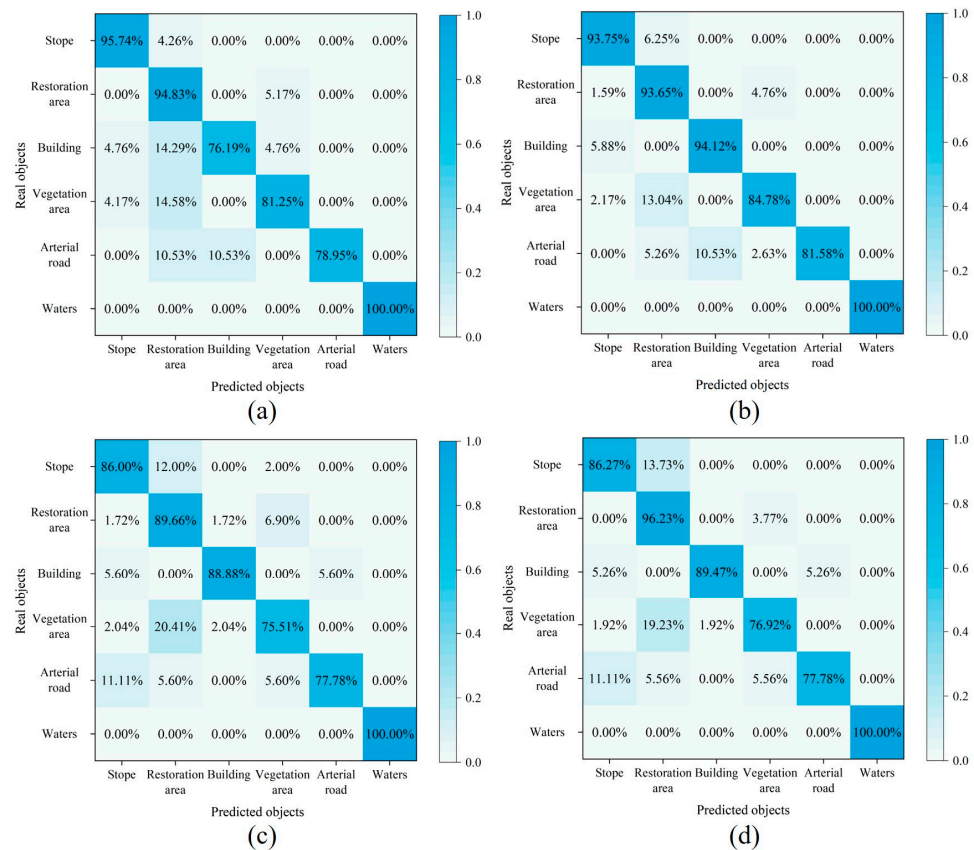


Figure 7. The three upper images, from left to right, show the segmentation scales 100, 285, and 400. The lower figure presents the image segmentation quality evaluation index chart.

### 3.2. Evaluation of Optimal Segmentation Results

To test the optimal segmentation scale, this study performed multi-scale segmentation of the UAV images at a scale of 360, keeping other parameters constant. A new RF model was also trained based on this and applied to the study area. Figure 8a displays the confusion matrix of the classification results. The diagonal values represent the recall rate of each class. The OA is 88.21%, and the Kappa is 0.8455. In comparison to the results obtained with an optimal segmentation scale of 285, the OA and Kappa decreased by 2.05% and 0.0262, respectively, indicating that the optimal segmentation scale significantly improves the object integrity, thereby improving classification accuracy.



**Figure 8.** Confusion matrix of the classification results. (a) The confusion matrix generated by the RF algorithm after multi-scale segmentation at a segmentation scale of 360; (b–d) are the confusion matrices generated by RF, SVM, and KNN algorithms, respectively, after optimal scale segmentation.

### 3.3. Evaluation of Features Importance

Regarding the land use classification of open-pit mines, different features have different impacts on the model performance. The importance of features is evaluated by the OOB error of RF. Figure 9 shows the optimal feature combination and importance ranking in this paper. The mean value of the green band in the spectral features ranks highest among all features, followed by the VDMI index in the index features. Although spectral and index features share comparable significance, the optimal feature combination slightly favors spectral features over index features, suggesting their marginally greater importance. In contrast, texture features, despite their variety, exhibit lower overall importance, with the highest-scoring GLCM\_Ctrst3 only reaching the fifth place. The proportion of texture features in the top 19 is low, indicating that their overall importance is lower than that of index features. Spatial features, totaling 13, rank relatively lower at the 7th, 15th, and 17th positions among the top 19 features, indicating their lesser importance. In summary, the

descending order of feature importance in this study is as follows: spectral features, index features, texture features, and spatial features.

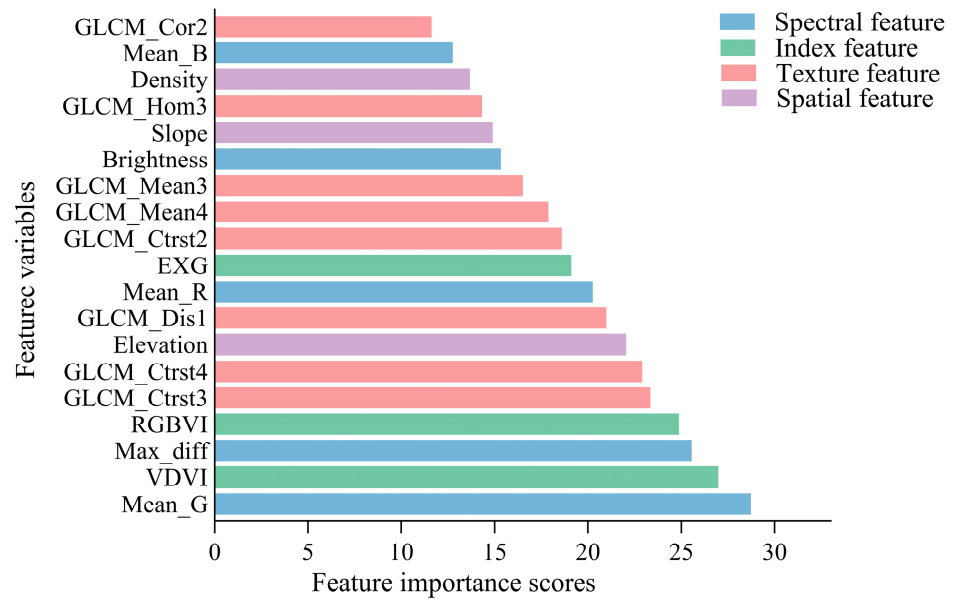


Figure 9. Feature importance ranking.

During model training, integrating multi-feature information can improve the robustness, reliability, and generalization ability of the model. However, increasing the number of features does not necessarily improve accuracy. Adding too many features can introduce information redundancy, which will affect the classification effect. Hence, this study employs a recursive feature elimination approach to select spectral, index, texture, and spatial features, aiming to achieve the optimal feature combination that can enhance classification accuracy. To study the correlation between the number of features and the OOB error, the OOB error was computed across various feature counts by sequentially removing the features with the lowest importance scores. The results are visually represented in Figure 10. As the feature count rises, the OOB error initially experiences a sharp decline, followed by slow increases and fluctuations. The OOB error reaches its minimum when the feature count hits 19. Therefore, this study selected the features with importance scores ranking from 1 to 19 as the optimal feature combination.

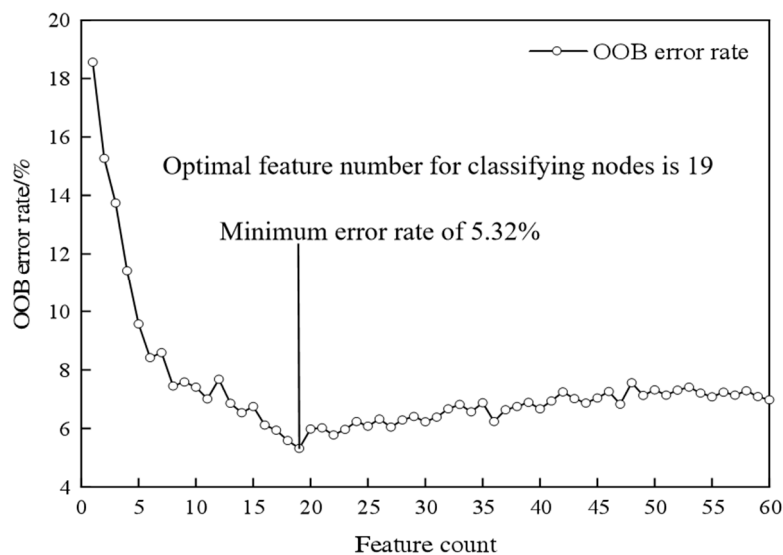
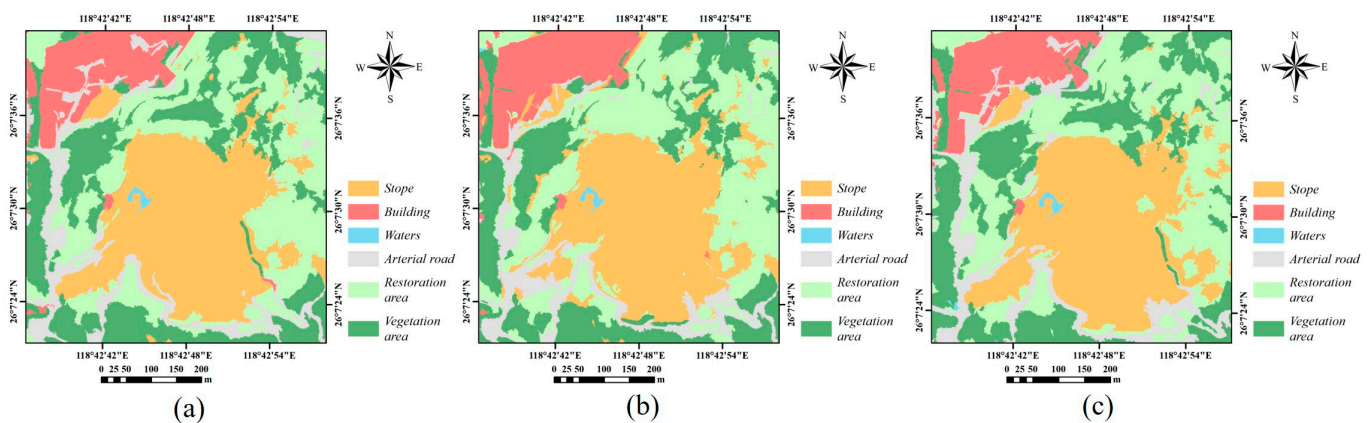


Figure 10. Correlation between the number of features and OOB error.

### 3.4. Evaluation of Classification Results

In order to evaluate the impacts of different classification methods on the performance of land use classification, this study compared the classification results of RF, SVM, and KNN algorithms based on the optimal feature combination (Figure 11). The results indicate that waters are primarily located in the central zone of the study area, covering a small area; the stopes are predominantly located in the middle region of the study area, exhibiting a continuous and expansive distribution; the restoration area and vegetation area are dispersed throughout the study area in an overlapping pattern; and buildings are predominantly situated in the northwest section of the study area, displaying a relatively clustered distribution. The classification results of SVM are more fragmented, with poor consistency in land feature distribution. KNN is able to recognize most buildings, and its overall classification performance is superior to SVM but inferior to RF.



**Figure 11.** Classification results of (a) RF, (b) SVM, and (c) KNN algorithms under optimal segmentation scale and optimal feature combination.

The classification results of the study area indicate that the RF algorithm outperforms the other two algorithms in terms of classification performance and can accurately identify most land use categories. The study area covers 37.75 hectares, including stope, restoration area, buildings, waters, natural vegetation, and arterial roads. The stope is the most widely distributed, covering an area of 10.98 hectares, accounting for 29.07% of the entire study area. The restoration area and the vegetation area cover an area of 10.34 hectares and 9.05 hectares, respectively, accounting for 27.38% and 23.97% of the study area. The area of the arterial roads (3.86 hectares) and buildings (3.45 hectares) is relatively small, accounting for 10.23% and 9.13% of the study area, respectively. Waters cover the smallest area, only 0.08 hectares, and is predominantly situated in the central region.

This study quantitatively examined the accuracy of land use classification utilizing confusion matrices. And an accuracy evaluation data are shown in Table 5. Figure 8b–d present the confusion matrices for RF, SVM, and KNN classifications, respectively. Compared to the SVM algorithm, the RF algorithm achieved improvements of 6.67% in OA and 0.0876 in Kappa, particularly excelling in identifying vegetation, arterial roads, and buildings. As evident from the classification results, the RF algorithm outperforms SVM in distinguishing between vegetated and non-vegetated areas. However, there is still room for improvement in identifying restoration and vegetation areas. The RF algorithm is able to recognize schools accurately, while the SVM and KNN algorithms have high misclassification rates, especially KNN. Additionally, RF has the highest accuracy rate in terms of main road recognition.

The confusion matrix accuracy evaluation table (Table 5) indicates that the RF algorithm exhibits superior classification performance, achieving an OA of 90.77% and a Kappa of 0.8786. In addition, the PA and UA of most categories exceed 84%. Compared to KNN and SVM, the RF algorithm has shown improvement in classification accuracy, demonstrat-

ing the effectiveness of this method in enhancing the accuracy of land use classification in open-pit mines.

**Table 5.** Accuracy evaluation of RF and SVM algorithms.

Classification Algorithm	Accuracy	Stope	Restoration Area	Building	Vegetation Area	Arterial Road	Waters
RF algorithm	PA/%	93.75	85.51	88.89	91.86	100	100
	UA/%	93.75	93.65	94.12	84.78	81.58	100
	OA/%	90.77					
	Kappa	0.8786					
SVM algorithm	PA/%	89.58	75.36	88.89	86.05	93.33	100
	UA/%	86.00	89.66	88.89	75.51	77.78	100
	OA/%	84.10					
	Kappa	0.791					
KNN algorithm	PA/%	91.67	73.91	94.44	93.02	93.33	100
	UA/%	86.27	96.23	89.47	76.92	77.78	100
	OA/%	86.15					
	Kappa	0.8189					

Based on the optimal feature combination, different algorithms were used for object-oriented classification. The misclassification and omission errors for each land use category are shown in Figure 12a,b, respectively. Among them, the misclassification errors for vegetation area and arterial roads are large, and the omission errors for restoration area, buildings, and vegetation area are large. Introducing multiple categories of features is beneficial for describing the characteristics of various land types from multiple perspectives, thereby reducing the errors of misclassification and omission. The RF algorithm exhibits relatively small misclassification and omission errors for various land use categories, whereas the SVM and KNN algorithms demonstrate larger classification errors for these categories. The results further confirm the superiority of the RF algorithm in dealing with high-dimensional features.

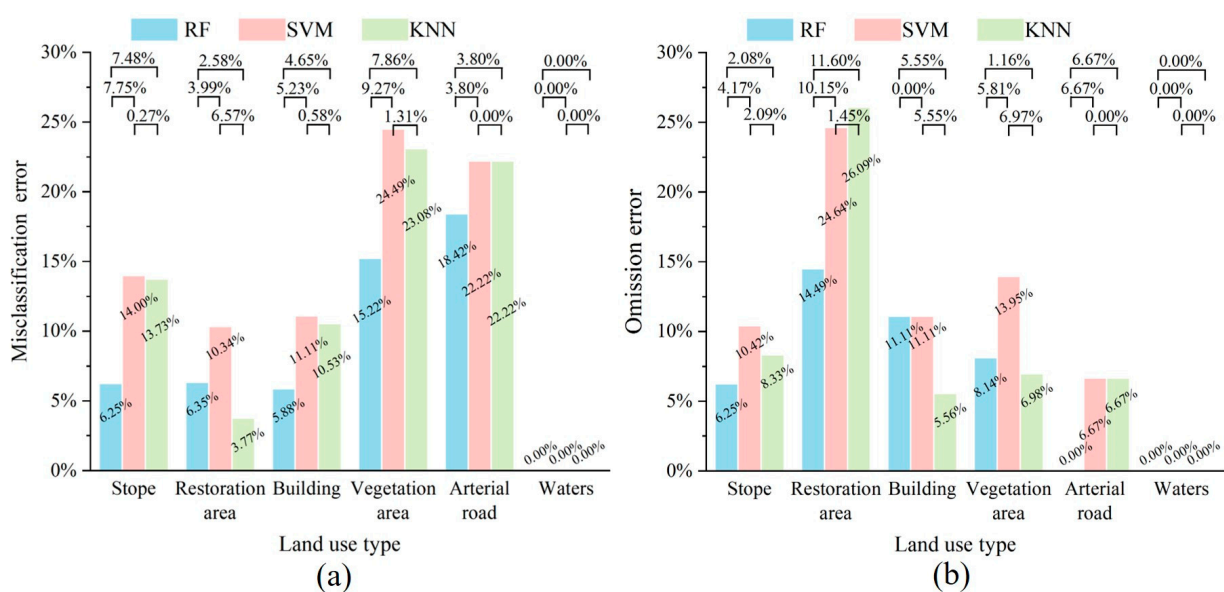


**Figure 12.** (a) Misclassification error and (b) omission error of different classification algorithms.

#### 4. Discussion

The classification results of different models reveal that the RF model outperforms both the KNN and SVM models, coinciding with the results of other studies [44–46]. The RF model derives the final classification result through a majority voting mechanism, effectively handling high-dimensional data and being insensitive to noise. With an OA > 90% and Kappa > 0.87, RF exhibits feasibility and high classification accuracy in land use classification for open-pit mines using low-altitude UAV imagery. The SVM performs well in binary classification but has limitations in multi-class classification [47]. The KNN is a simple, intuitive, and easily implementable classification algorithm that primarily relies on the similarity between training samples and test samples for classification [48]. However, KNN is prone to misclassification and omission when faced with high computational loads and imbalanced sample distributions. Therefore, the RF algorithm, with its robust resistance to overfitting and parallel processing capabilities, continues to exhibit favorable classification performance in complex open-pit mining scenarios. Apart from machine learning, artificial neural networks (ANNs) are also widely used algorithms for land use classification, but numerous studies have indicated that RF typically demonstrates greater accuracy compared to ANNs in classifications involving small areas and limited samples [49,50].

In open-pit mines, stopes, buildings, and waters are relatively easy to identify, whereas restoration areas, vegetation areas, and arterial roads are not easily distinguishable. Due to their small size and distinct spectral characteristics, the waters within the study area exhibit high classification accuracy across various algorithms. The classification accuracy for stopes and buildings is generally high, but they are prone to being misclassified due to their high similarity with arterial roads. Restoration areas were not easily recognized, mainly due to the fact that some areas were overexposed by excessive sunlight. In addition, KNN and SVM algorithms performed poorly in classifying the classification accuracy of restoration areas and vegetation areas, primarily due to the spectral features between them, which often results in the misclassification of restoration areas as vegetation areas. The PA of the arterial roads exceeded 90% for all classification algorithms, but the UA is relatively low, primarily due to the misclassification of stopes, restoration areas, and buildings as arterial roads. Overall, the RF algorithm demonstrates higher classification accuracy in stopes, restoration areas, vegetation areas, and arterial roads; especially in restoration areas, the RF algorithm achieves a significant improvement in PA by 10.15% and 11.60% compared to the SVM and KNN algorithms, respectively.

This study identified spectral features as the most critical for land use classification, preceded by index features. In contrast, texture and spatial features, particularly spatial ones, hold a relatively minor significance. In this study, index, texture, and spatial features are added to the spectral features to enrich the object information and improve the classification accuracy. Nonetheless, empirical evidence suggests that an increase in the number of features does not invariably result in enhanced classification accuracy. Once the number of features reaches a saturation point, further additions may not significantly improve the separability of the categories but may lead to overfitting, thereby potentially compromising the classification performance. To maximize the classification accuracy, it is recommended to use feature importance ranking and the RFE method to construct an optimal feature combination, which not only reduces the computational cost but also significantly enhances classification efficiency.

The analysis of algorithm accuracy shows that the RF algorithm based on the optimal segmentation scale and optimal feature combination achieved the highest OA and Kappa. This may be attributed to the following points: (1) Using the optimal segmentation scale evaluation model can improve the object purity and boundary clarity. (2) The RF algorithm randomly selects feature subsets for splitting when constructing decision trees, reducing the risk of overfitting. When the optimal segmentation scale and optimal feature combination are adopted, this advantage is further amplified. (3) Although the spectral features of UAV images are less than those of satellite remote sensing imagery, the combination of

index, texture, and spatial features can effectively improve the classification accuracy. (4) Reducing the number of feature combinations from the original 58 to 19 minimizes the OOB error to 5.32%, simplifies the model, and improves the classification efficiency.

## 5. Conclusions

This current study selects an open-pit mine in Fuzhou City, Fujian Province, China, as the research area and proposes an open-pit mine land use classification method that integrates an object-oriented method with the RF algorithm based on UAV images. The results indicated that after switching from a segmentation scale of 360 to an optimal segmentation scale, the OA increased from 88.21% to 90.77%, indicating that optimal scale segmentation can significantly improve classification accuracy. After using the optimal feature combination, the OOB error of RF was reduced to a minimum, indicating that it is necessary to select the most suitable feature combination to assist classification. The results indicate that the RF algorithm significantly improves classification accuracy compared to the KNN and SVM algorithms, indicating that this method can be prioritized for land use classification in small sample and small area open-pit mines. However, this study only obtained visible imagery of the mines, which has relatively limited diversity. In addition, the processing of the illumination conditions of the images is still insufficient. Subsequent research can be expanded to multispectral or hyperspectral imagery of the mines and integrate an image processing algorithm with better illumination adaptability.

UAVs offer distinct advantages in remote sensing monitoring due to their portability, high mobility, efficient data processing capabilities, and ability to provide high-resolution imagery. These advantages make high-resolution UAV imagery a promising alternative to traditional ground surveys and satellite remote sensing methods. However, UAVs also encounter some challenges in practical applications, such as large volumes of image data, resolution loss during multi-image stitching, and limited battery life. Therefore, high-resolution UAV imagery is suitable for land use classification in small-area open-pit mines and holds vast potential in monitoring and managing open-pit mines.

**Author Contributions:** Conceptualization, Y.H. and Y.L.; methodology, Y.H. and Y.L.; validation, B.C.; formal analysis, Y.L. and B.C.; resources, Y.L.; data curation, B.C., Y.C., and X.Y.; writing—original draft preparation, Y.H., Y.L., and Z.X.; writing—review and editing, Y.L., B.C., Y.C., and M.L.; supervision, Y.H. All authors have read and agreed to the published version of the manuscript.

**Funding:** Funding was provided by the Fujian Province's Foreign Cooperation Project in 2023 (2023I0047), the Fujian Provincial Natural Science Foundation Project (2023J011432), the Ministry of Education's supply-demand docking employment and education project (2024011223947), the Open Project Fund of Hunan Provincial Key Laboratory for Remote Sensing Monitoring of Ecological Environment in Dongting Lake Area (Project No: DTH Key Lab. 2022-04; DTH Key Lab. 2024-04), the Fujian Provincial Natural Science Foundation Guiding Project (2024Y0057), the Fujian Province Social Science Plan Project (FJ2024BF071), and the Natural Science Foundation of Fujian Province, China Grants (2024J011195).

**Data Availability Statement:** Original data are available at <https://doi.org/10.17605/OSF.IO/4FR5H>, accessed on 19 November 2024.

**Acknowledgments:** The authors would like to express their sincere gratitude to all the staff of the Digital Fujian Institute of Big Data for Natural Disaster Monitoring and the Minerals Editorial Board for their support of this paper.

**Conflicts of Interest:** The authors declare no conflicts of interest.

## References

1. Hu, Z.; Li, Y.; Li, G.; Han, J.; Liu, S. Opportunities and Challenges of Land Reclamation and Ecological Restoration in Mining Areas under the Goal of Carbon Neutrality. *Coal Sci. Technol.* **2023**, *51*, 474–483. [[CrossRef](#)]
2. Jurakulov, S. Impact of the Mining Industry on People and the Environment. *Theor. Asp. Form. Pedagog. Sci.* **2023**, *2*, 143–150.
3. Shahmoradi, J.; Talebi, E.; Roghanchi, P.; Hassanalian, M. A Comprehensive Review of Applications of Drone Technology in the Mining Industry. *Drones* **2020**, *4*, 34. [[CrossRef](#)]



4. Sengupta, M. *Environmental Impacts of Mining: Monitoring, Restoration, and Control*, 2nd ed.; CRC Press: Boca Raton, FL, USA, 2021; ISBN 978-1-00-316401-2.
5. Abebe, G.; Getachew, D.; Ewunetu, A. Analysing Land Use/Land Cover Changes and Its Dynamics Using Remote Sensing and GIS in Gubalafito District, Northeastern Ethiopia. *SN Appl. Sci.* **2021**, *4*, 30. [[CrossRef](#)]
6. Alhassan, V.; Henry, C.; Ramanna, S.; Storie, C. A Deep Learning Framework for Land-Use/Land-Cover Mapping and Analysis Using Multispectral Satellite Imagery. *Neural Comput. Appl.* **2020**, *32*, 8529–8544. [[CrossRef](#)]
7. Gudmann, A.; Csikós, N.; Szilassi, P.; Mucsi, L. Improvement in Satellite Image-Based Land Cover Classification with Landscape Metrics. *Remote Sens.* **2020**, *12*, 3580. [[CrossRef](#)]
8. Myint, S.W.; Gober, P.; Brazel, A.; Grossman-Clarke, S.; Weng, Q. Per-Pixel vs. Object-Based Classification of Urban Land Cover Extraction Using High Spatial Resolution Imagery. *Remote Sens. Environ.* **2011**, *115*, 1145–1161. [[CrossRef](#)]
9. Akar, O.; Gormus, E.T. Land Use/Land Cover Mapping from Airborne Hyperspectral Images with Machine Learning Algorithms and Contextual Information. *Geocarto Int.* **2022**, *37*, 3963–3990. [[CrossRef](#)]
10. Hu, S.; He, X.; Tian, Z. A High-Score Remote Sensing Imagery Land Use Classification Method Based on MLUM-Net. *Comput. Sci.* **2023**, *50*, 161–169.
11. Mitchell, A.L.; Rosenqvist, A.; Mora, B. Current Remote Sensing Approaches to Monitoring Forest Degradation in Support of Countries Measurement, Reporting and Verification (MRV) Systems for REDD+. *Carbon Balance Manag.* **2017**, *12*, 9. [[CrossRef](#)]
12. Shaik, R.U.; Periasamy, S.; Zeng, W. Potential Assessment of PRISMA Hyperspectral Imagery for Remote Sensing Applications. *Remote Sens.* **2023**, *15*, 1378. [[CrossRef](#)]
13. Fahlstrom, P.G.; Gleason, T.J.; Sadraey, M.H. *Introduction to UAV Systems*; John Wiley & Sons: Hoboken, NJ, USA, 2022; ISBN 978-1-119-80261-7.
14. Fu, X.; Lu, H.; Zhu, Q.; Liu, T.; Gou, S. Dynamic Monitoring of Land Use Information in Mountainous Areas by Using UAV Images. *Mt. Res.* **2016**, *34*, 121–126. [[CrossRef](#)]
15. Zhang, Z.; Zhao, X.; Jiang, H.; Yuan, H.; Yang, L.; Gao, X.; Shi, L.; Niu, Y. Accurate Land Use Classification in the Weibei Dry Loess Plateau Area Based on UAV Imagery and Deep Learning. *Trans. Chin. Soc. Agric. Eng.* **2022**, *38*, 199–209.
16. Li, J.; Hong, D.; Gao, L.; Yao, J.; Zheng, K.; Zhang, B.; Chanussot, J. Deep Learning in Multimodal Remote Sensing Data Fusion: A Comprehensive Review. *Int. J. Appl. Earth Obs. Geoinf.* **2022**, *112*, 102926. [[CrossRef](#)]
17. Maus, V.; Giljum, S.; Gutschlhofer, J.; da Silva, D.M.; Probst, M.; Gass, S.L.B.; Luckeneder, S.; Lieber, M.; McCallum, I. A Global-Scale Data Set of Mining Areas. *Sci. Data* **2020**, *7*, 289. [[CrossRef](#)]
18. Hu, W. *Urban Flooding Vulnerability Assessment and Spatial and Temporal Heterogeneity Study*; Beijing University of Civil Engineering and Architecture: Beijing, China, 2024.
19. Lv, Z.; Liu, T.; Benediktsson, J.A. Object-Oriented Key Point Vector Distance for Binary Land Cover Change Detection Using VHR Remote Sensing Images. *IEEE Trans. Geosci. Remote Sens.* **2020**, *58*, 6524–6533. [[CrossRef](#)]
20. Lu, Z.; Qi, L.; Zhang, H.; Wan, J.; Zhou, J. Image Segmentation of UAV Fruit Tree Canopy in a Natural Illumination Environment. *Agriculture* **2022**, *12*, 1039. [[CrossRef](#)]
21. Zhang, J.; Lin, S.; Ding, L.; Bruzzone, L. Multi-Scale Context Aggregation for Semantic Segmentation of Remote Sensing Images. *Remote Sens.* **2020**, *12*, 701. [[CrossRef](#)]
22. Chen, Y. An Analytical Process of Spatial Autocorrelation Functions Based on Moran's Index. *PLoS ONE* **2021**, *16*, e0249589. [[CrossRef](#)]
23. Yan, C.; Fan, X.; Fan, J.; Wang, N. Improved U-Net Remote Sensing Classification Algorithm Based on Multi-Feature Fusion Perception. *Remote Sens.* **2022**, *14*, 1118. [[CrossRef](#)]
24. Li, D.; Miao, Y.; Gupta, S.K.; Rosen, C.J.; Yuan, F.; Wang, C.; Wang, L.; Huang, Y. Improving Potato Yield Prediction by Combining Cultivar Information and UAV Remote Sensing Data Using Machine Learning. *Remote Sens.* **2021**, *13*, 3322. [[CrossRef](#)]
25. Elazab, A.; Bort, J.; Zhou, B.; Serret, M.D.; Nieto-Taladriz, M.T.; Araus, J.L. The Combined Use of Vegetation Indices and Stable Isotopes to Predict Durum Wheat Grain Yield under Contrasting Water Conditions. *Agric. Water Manag.* **2015**, *158*, 196–208. [[CrossRef](#)]
26. Woebbecke, D.M.; Meyer, G.E.; Von Bargaen, K.; Mortensen, D.A. Color Indices for Weed Identification Under Various Soil, Residue, and Lighting Conditions. *Trans. ASAE* **1995**, *38*, 259–269. [[CrossRef](#)]
27. Bendig, J.; Yu, K.; Aasen, H.; Bolten, A.; Bennertz, S.; Broscheit, J.; Gnyp, M.L.; Bareth, G. Combining UAV-Based Plant Height from Crop Surface Models, Visible, and near Infrared Vegetation Indices for Biomass Monitoring in Barley. *Int. J. Appl. Earth Obs. Geoinf.* **2015**, *39*, 79–87. [[CrossRef](#)]
28. Wang, Y.; Yin, D.; Lou, L.; Li, X.; Cheng, P.; Huang, Y. Luotuo Mountain Waste Dump Cover Interpretation Combining Deep Learning and VDVI Based on Data from an Unmanned Aerial Vehicle (UAV). *Remote Sens.* **2022**, *14*, 4043. [[CrossRef](#)]
29. Zebari, R.; Abdulazeez, A.; Zeebaree, D.; Zebari, D.; Saeed, J. A Comprehensive Review of Dimensionality Reduction Techniques for Feature Selection and Feature Extraction. *JASTT* **2020**, *1*, 56–70. [[CrossRef](#)]
30. Lv, Z.; Zhang, P.; Sun, W.; Benediktsson, J.A.; Li, J.; Wang, W. Novel Adaptive Region Spectral–Spatial Features for Land Cover Classification With High Spatial Resolution Remotely Sensed Imagery. *IEEE Trans. Geosci. Remote Sens.* **2023**, *61*, 5609412. [[CrossRef](#)]
31. Zhang, T.; Su, J.; Xu, Z.; Luo, Y.; Li, J. Sentinel-2 Satellite Imagery for Urban Land Cover Classification by Optimized Random Forest Classifier. *Appl. Sci.* **2021**, *11*, 543. [[CrossRef](#)]

32. Jeon, H.; Oh, S. Hybrid-Recursive Feature Elimination for Efficient Feature Selection. *Appl. Sci.* **2020**, *10*, 3211. [[CrossRef](#)]
33. Talaei Khoei, T.; Kaabouch, N. A Comparative Analysis of Supervised and Unsupervised Models for Detecting Attacks on the Intrusion Detection Systems. *Information* **2023**, *14*, 103. [[CrossRef](#)]
34. Guo, Q.; Zhang, J.; Guo, S.; Ye, Z.; Deng, H.; Hou, X.; Zhang, H. Urban Tree Classification Based on Object-Oriented Approach and Random Forest Algorithm Using Unmanned Aerial Vehicle (UAV) Multispectral Imagery. *Remote Sens.* **2022**, *14*, 3885. [[CrossRef](#)]
35. Josso, P.; Hall, A.; Williams, C.; Le Bas, T.; Lusty, P.; Murton, B. Application of Random-Forest Machine Learning Algorithm for Mineral Predictive Mapping of Fe-Mn Crusts in the World Ocean. *Ore Geol. Rev.* **2023**, *162*, 105671. [[CrossRef](#)]
36. Schonlau, M.; Zou, R.Y. The Random Forest Algorithm for Statistical Learning. *Stata J.* **2020**, *20*, 3–29. [[CrossRef](#)]
37. Vasić, M.V.; Jantunen, H.; Mijatović, N.; Nelo, M.; Muñoz Velasco, P. Influence of Coal Ashes on Fired Clay Brick Quality: Random Forest Regression and Artificial Neural Networks Modeling. *J. Clean. Prod.* **2023**, *407*, 137153. [[CrossRef](#)]
38. Zhang, F.; Lv, L.; Han, L.; Liu, D.; Fan, T. Structured Least Squares Twinned Support Vector Machines for Intuition Fuzzy. *J. Appl. Sci.* **2024**, *42*, 350–363.
39. Pokorný, T.; Vrba, J.; Fiser, O.; Vrba, D.; Drizdal, T.; Novak, M.; Tosi, L.; Polo, A.; Salucci, M. On the Role of Training Data for SVM-Based Microwave Brain Stroke Detection and Classification. *Sensors* **2023**, *23*, 2031. [[CrossRef](#)]
40. Xing, W.; Bei, Y. Medical Health Big Data Classification Based on KNN Classification Algorithm. *IEEE Access* **2020**, *8*, 28808–28819. [[CrossRef](#)]
41. Ge, G.; Shi, Z.; Zhu, Y.; Yang, X.; Hao, Y. Land Use/Cover Classification in an Arid Desert-Oasis Mosaic Landscape of China Using Remote Sensed Imagery: Performance Assessment of Four Machine Learning Algorithms. *Glob. Ecol. Conserv.* **2020**, *22*, e00971. [[CrossRef](#)]
42. Zhang, L.; Liu, Z.; Ren, T.; Liu, D.; Ma, Z.; Tong, L.; Zhang, C.; Zhou, T.; Zhang, X.; Li, S. Identification of Seed Maize Fields With High Spatial Resolution and Multiple Spectral Remote Sensing Using Random Forest Classifier. *Remote Sens.* **2020**, *12*, 362. [[CrossRef](#)]
43. Luo, C.; Qi, B.; Liu, H.; Guo, D.; Lu, L.; Fu, Q.; Shao, Y. Using Time Series Sentinel-1 Images for Object-Oriented Crop Classification in Google Earth Engine. *Remote Sens.* **2021**, *13*, 561. [[CrossRef](#)]
44. Islam, N.; Rashid, M.M.; Wibowo, S.; Xu, C.-Y.; Morshed, A.; Wasimi, S.A.; Moore, S.; Rahman, S.M. Early Weed Detection Using Image Processing and Machine Learning Techniques in an Australian Chilli Farm. *Agriculture* **2021**, *11*, 387. [[CrossRef](#)]
45. Ye, Z.; Guo, Q.; Zhang, J.; Zhang, H.; Deng, H. Extraction of urban impervious surface based on the visible images of UAV and OBIA-RF algorithm. *Trans. Chin. Soc. Agric. Eng.* **2022**, *38*, 225–234. [[CrossRef](#)]
46. Zhou, R.; Yang, C.; Li, E.; Cai, X.; Yang, J.; Xia, Y. Object-Based Wetland Vegetation Classification Using Multi-Feature Selection of Unoccupied Aerial Vehicle RGB Imagery. *Remote Sens.* **2021**, *13*, 4910. [[CrossRef](#)]
47. Zhang, D.; Li, D.; Zhou, L.; Wu, J. Fine Classification of UAV Urban Nighttime Light Images Based on Object-Oriented Approach. *Sensors* **2023**, *23*, 2180. [[CrossRef](#)] [[PubMed](#)]
48. Du, H.; Li, M.; Xu, Y.; Zhou, C. An Ensemble Learning Approach for Land Use/Land Cover Classification of Arid Regions for Climate Simulation: A Case Study of Xinjiang, Northwest China. *IEEE J. Sel. Top. Appl. Earth Obs. Remote Sens.* **2023**, *16*, 2413–2426. [[CrossRef](#)]
49. Talukdar, S.; Singha, P.; Mahato, S.; Shahfahad, Pal, S.; Liou, Y.-A.; Rahman, A. Land-Use Land-Cover Classification by Machine Learning Classifiers for Satellite Observations—A Review. *Remote Sens.* **2020**, *12*, 1135. [[CrossRef](#)]
50. Kasahun, M.; Legesse, A. Machine Learning for Urban Land Use/ Cover Mapping: Comparison of Artificial Neural Network, Random Forest and Support Vector Machine, a Case Study of Dilla Town. *Heliyon* **2024**, *10*, e39146. [[CrossRef](#)]

**Disclaimer/Publisher’s Note:** The statements, opinions and data contained in all publications are solely those of the individual author(s) and contributor(s) and not of MDPI and/or the editor(s). MDPI and/or the editor(s) disclaim responsibility for any injury to people or property resulting from any ideas, methods, instructions or products referred to in the content.